Soft Matter

Accepted Manuscript

ROYAL SOCIETY OF CHEMISTRY

www.rsc.org/softmatter

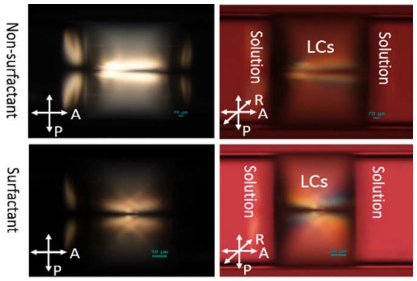

Liquid crystals confined in microcapillaries for imaging chemoresponsive interfacial phenomena.

Soft Matter

ARTICLE

Nematic Liquid Crystals Confined in Microcapillaries for Imaging Phenomena at Liquid-Liquid Interfaces

Received 00th January 20xx,
Accepted 00th January 20xx

DOI: 10.1039/x0xx00000x

www.rsc.org/

Shenghong Zhong and Chang-Hyun Jang*

Here, we report development of an experimental system based on liquid crystals (LCs) confined in microcapillaries for imaging interfacial phenomena. The inner surfaces of the microcapillaries were modified with octadecyltrichlorosilane to promote an escaped radial configuration of LCs. We checked the optical appearance of the capillary-confined LCs under a crossed polarizing microscope and determined their arrangement based on side and top views. We then placed the capillary-confined LCs in contact with non-surfactant and surfactant solutions, producing characteristic textures of two bright lines and a four-petal shape, respectively. We also evaluated the sensitivity, stability, and reusability of the system. Our sensing system was more sensitive than previously reported LC thin film systems. The textures formed in the microcapillary were stable for more than 120 h and the capillary could be reused at least 10 times. Finally, we successfully applied our system to image the interactions of phospholipids and bivalent metal ions. In summary, we developed a simple, small, portable, sensitive, stable, and reusable experimental system that can be broadly applied to monitor liquid-liquid interfacial phenomena. These results provide valuable information for designs using confined LCs as chemoresponsive materials in optical sensors.

1 Introduction

Liquid crystals (LCs) are a fascinating class of soft matter between an isotropic liquid and a crystalline state. LCs offer tremendous potential for fundamental science and innovative applications due to their characteristic properties like fluidity, elasticity, optical anisotropy, long-range order, and simple alignment on a substrate, as well as being easily controlled and adaptable to a wide range of designs. Beyond their highly successful applications in displays, LCs have opened up diverse new and exciting lines of research and applications, including LC organic electronics[1], LC lasers[2], LC photonics[3], LC fibers[4], LC block copolymers[5], colloids in LCs[6], active LCs[7–9], LC microfluidics[10], LC soft lithography[11], LC skyrmion lattices[12], and LC-based sensors[13–15].

The concept of LC sensors at liquid-liquid interfaces was first reported by Brake et al.[16], in which they developed an experimental system to report reversible adsorption of amphiphiles at aqueous-LC interfaces. Due to its many advantages, such as easy fabrication, high sensitivity, rapid response, label-free nature, visibility to the naked eye, and lack of complex instrumentation[17], this system has been broadly applied for reporting interfacial phenomena at liquid-liquid interfaces. One example of a well-developed application is LC thin film chemical and biological sensors. Numerous sensing applications based on LC thin films have been reported, including for proteins[18], enzymes[19-21], DNA[22], glucose[13], phospholipids[17], fatty acids[23], and heavy metals[24]. Although LC thin films are simple and sensitive and their transmission electron microscopy (TEM) grids can easily be modified by functional groups, there are challenges that can be improved upon. Among these, size reduction would be desirable. Optical cells of LC thin film system are typically fabricated on a glass slide fixed at the bottom of an eight-well chamber with a size of approximately 7.5 cm × 2.5 cm × 1.5 cm (length × width × height). Thus, each experiment requires a chamber with a volume of 3.5 cm^3. Generally, hundreds of microliters of solution are needed for imaging; therefore, the system cannot be used to detect trace amounts of substances. When preparing the LC thin films on the TEM grids, excess LC is removed, wasting experimental materials. The TEM grid is not actually needed for imaging as it is only used to anchor the LCs. In addition, the TEM grid is easily deformed and oxidized, limiting reusability. Because the chamber is open to the environment, LC-aqueous interfaces can be disturbed by air flow, heat, and certain mechanical vibrations.

There is another imaging system based on LC droplets on solid surfaces, which was established by Hu and Jang[25]. This system can spontaneously form LC droplet patterns at micrometer-scale. This system hold great sensitivity and can be easily fabricated. Due to the small amount of solutions of interests, typically, this system can keep stable for only a few minutes, which limited its applications.

Department of Chemistry, Gachon University, Seongnam-Si, Gyeonggi-Do, 461-701, Korea. E-mail: chjang4u@gachon.ac.kr
See DOI: 10.1039/x0xx00000x

Here we report the development of a new experimental imaging system based on nematic liquid crystals confined in microcapillaries, which compared to LC thin film system is smaller, more stable, reusable, portable, and easily fabricated. We initially studied the birefringence and ordering configuration of the nematic LCs confined in the microcapillaries. Adsorption of amphiphiles at the LC-water interface and their influence on ordering was also evaluated. The performance (sensitivity, stability, and reusability) of this novel imaging system was researched. Finally, we used this system for an actual imaging application, monitoring interactions between phospholipid vesicles and bivalent metal ions.

2 Experimental

2.1 Materials

Nematic liquid crystal 4-cyano-4'-pentylbiphenyl (5CB) was purchased from EM industries (Hawthorne, NY). n-Heptane (anhydrous) was purchased from Daejung Chemicals & Metals Co., Ltd. (South Korea). Sulfuric acid, hydrogen peroxide (30% w/v), phosphate-buffered saline (PBS) (10 mM phosphate, 138 mM NaCl, 2.7 mM KCl; pH 7.4), octadecyltrichlorosilane (OTS), sodium hydroxide, hydrochloric acid, microcapillaries (5 µL), iron (II) sulfate heptahydrate, calcium chloride, cobalt (II) chloride hexahydrate, copper (II) nitrate hydrate, magnesium chloride, lead (II) nitrate, 1,2-distearoyl-*sn*-glycero-3-phospho-*rac*-(1-glycerol) sodium salt (DOPG), sodium oleate, hexadecyl trimethyl ammonium bromide (CTAB), and sodium dodecyl sulfate (SDS) were purchased from Sigma-Aldrich (St. Louis, MO). All aqueous solutions were prepared with deionized (DI) water (18.2 MΩ·cm^{-1}) using a Milli-Q water purification system (Millipore, Bedford, MA).

2.2 Treatment of microcapillaries with octadecyltrichlorosilane

The microcapillaries were cleaned using piranha solution (70% H_2SO_4:30% H_2O_2) for 30 min at 80 °C (caution: piranha solution reacts violently with organic materials and should be handled with extreme care; do not store the solution in a closed container). The microcapillaries were then rinsed with water, ethanol, and methanol and dried under a stream of gaseous N_2, after which they were heated to 120 °C overnight prior to OTS deposition. The piranha-cleaned microcapillaries were immersed in an OTS:n-heptane solution (120 µL:80 mL) for 30 min at room temperature, after which they were rinsed with methylene chloride and dried under N_2.

2.3 Preparation of phospholipid vesicles

DOPG solution was prepared as previously reported[26]. Briefly, DOPG dissolved in chloroform (50 mg·mL^{-1}) was dried under a stream of N_2 and desiccated under vacuum for at least 3 h. The dried DOPG was then resuspended with PBS solution (pH = 5.8) to a DOPG concentration of 2 mM.

2.4 Reaction of bivalent metal ions and phospholipid vesicles

Phospholipid vesicles (100 µL, 2 mM) were added to a 1.2-mL solution of bivalent metal ion (10 mM). The final concentration of phospholipid in the mixture was about 150 µM. The mixture was shaken for about 1 min and used immediately after preparation.

2.5 Preparation of the microcapillary-confined liquid crystal imaging platform

About 0.5 µL of 5CB was siphoned into one end of a microcapillary via contact. The aqueous solution of interest was then injected into the capillary using a syringe whose needle was connected to a soft micropipe. The liquid crystals automatically divided into several individual droplets, with both ends of the droplets contacting aqueous solution. The preparation of this imaging platform was illustrated in Scheme 1.

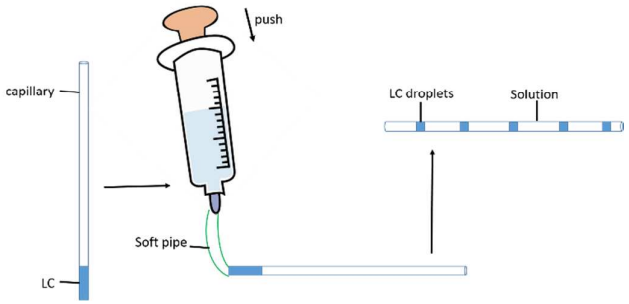

Scheme 1. The illustration of how to prepare micro-capillary confined LC imaging platform

2.6 Optical characterization of liquid crystal ordering

A polarized light microscope (Eclipse LV100POL; Nikon, Tokyo, Japan) was used to capture images of the optical textures observed by polarized light transmitted through the LC micro-droplets. Images were obtained using various objective lenses between crossed polarizers and the size was determined by comparison to the scale bar shown in the figure. All images were taken with a digital camera (DS-2Mv; Nikon) mounted on the microscope at a resolution of 1600 × 1200 pixels, a gain of 1.00×, and a shutter speed of 1/10 s.

3 Results and Discussion

3.1 Nematic liquid crystals confined in octadecyltrichlorosilane-treated microcapillaries

The inner surfaces of the microcapillaries were treated with OTS to control the alignment of the nematic LCs. In addition, the hydrophobicity of the OTS-treated microcapillary surface facilitated siphoning of 5CB into the microcapillary. After 5CB was added, we examined the LC optical properties under a crossed polarizing microscope (Figure 1A). A full wave retardation plate was also used to determine the configuration of the nematic director (Figure 1B). Schematics of side and top views are shown in Figure 1D and 1E, respectively. Based on the polarized microscopy (Figure 1A), the inner diameter of the

microcapillary was about 400 µm. At the center of the microcapillary, we observed a straight dark line, indicating a defect line. The insert shows the area highlighted by the red rectangle, showing that the width of the defect line was around 20 µm. On either side of the dark defect line there were two bright lines. We inserted a full wave retardation plate at a 45° angle to the polarizer and analyzer (Figure 1B, letter R) to determine the ordering configuration of the bright areas. The retardation plate added a fixed optical path difference (λ = 530 nm, green region) to each wavefront in the field. When there was no birefringent specimen in the optical path, the green wavelength band was adsorbed by the retardation plate, yielding bright magenta-red, representing a combination of all visible light spectral colors other than the green wavelength band. When a birefringent specimen was parallel to the plate, the relative retardation of the orthogonal wavefronts increased across the viewfield so that the color was shifted to longer wavelengths, absorbing red and showing a blue image. Otherwise, if a birefringent specimen was perpendicular to the plate, the relative retardation of the orthogonal wavefronts decreased so that the color was shifted to shorter wavelengths, absorbing blue and showing a yellow image. Thus, the color indicates the angle between the local director **n** of the LC and the retardation plate (R). If **n** is parallel to R, a blue color is observed, while an orange color indicates that **n** is perpendicular to R. The two bright lines have a faint blue-ish color above and an orange color below (Figure 1B); therefore, the director **n** was parallel and perpendicular to R, respectively (Figure 1E). This ordering configuration is also evident in Figure 1C, in which the capillary was rotated by 45°—the initially dark area in Figure 1A became bright and the previously bright area turned dark. Figure 1D shows that a defect formed in the center because the inner surface of the capillary was treated with OTS, which promoted a perpendicular alignment of the LCs into an escaped radial configuration. Figure 1E shows the alignment of the LCs from above, confirming the optical appearance in Figure 1A–C.

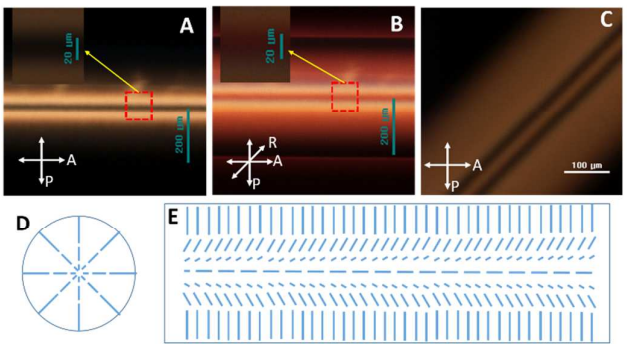

Figure 1. (A) Polarized microscope image of microcapillary-confined LCs (the insert shows a magnification of the defect line), (B) polarized microscope image with a full wave retardation plate inserted, (C) polarized microscope image with the capillary angled at 45°, (D) schematic of the side view of the LC configuration, and (E) schematic of the top view showing the alignment of the microcapillary-confined LCs.

3.2 Interactions between the microcapillary-confined nematic liquid crystals and solutions

After about 0.5 µL of the LC was siphoned into the microcapillary, the solution of interest was injected into the same end of the microcapillary. The solution mixed with the LC and propelled it to the other end of the capillary. A few minutes later, the solution and LC separated due to immiscibility and the LC divided into several individual droplets with a typical length of 300–500 µm (37–61 nL). Shortly, the stable optical images formed. We studied the optical textures of the LCs after contact with two different types of solutions (surfactant and non-surfactant solutions). We used deionized water and PBS solution as the non-surfactant solutions. When a single droplet of 5CB contacted the non-surfactant solutions, the optical appearance did not change substantially. The blue-ish color was clearer, and was below the orange color, which lead a reversed alignment (Figure 2C) from pure confined LC (Figure 1E). It is still not clear why sometimes blue color was above orange color, while sometimes blue color was below orange color. There were still two bright lines separated by one dark line (Figure 2A and 2B). However, the optical appearance at the LC-aqueous interface was different from that of the inner part of the LC droplet, due to perturbation of the LC by the solution.

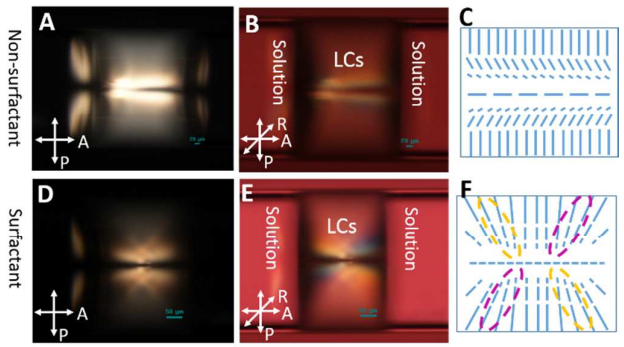

Figure 2. (A), (B), and (C) are the optical images and top view schematic of the microcapillary-confined LCs contacting the non-surfactant solutions; (D), (E), and (F) show the optical response and top view schematic of the microcapillary-confined LCs contacting the surfactant solutions. The purple and orange dashed circles in (F) indicate how the four-petal shape is formed.

When the LC contacted the 10 mM surfactant solutions (SDS, CTAB, and sodium oleate), a more interesting result occurred. In the crossed polarizers (Figure 2D), we still observed the dark defect line; however, the bright areas were no longer two straight lines, but four petal-shaped areas. We then inserted the full wave retardation plate to determine the ordering configuration of these LCs. Two of the four petals were blue, while the other two were orange (Figure 2E). In the blue areas, the local director **n** was parallel to the retardation plate R, while in the orange areas, the local director **n** was perpendicular to R. Thus, we determined the alignment of the LCs as shown in Figure 2F. The purple dashed circles represent the areas in which the local director was parallel to R, while the orange dashed circles indicate the areas in which the local

director **n** was perpendicular to R, together giving the four-petal appearance. The four-petal texture resulted from hybrid-alignment boundary conditions. The OTS aligned the LCs normal to the capillary, resulting in a radial orientation; however, the surfactant solution anchored the LCs along the capillary, producing a horizontal orientation. In the areas near the capillary surface, the OTS dominated the alignment, while in the areas near the LC-aqueous interface, the surfactant determined the LC orientation.

3.3 Performance of the microcapillary-confined liquid crystal imaging system

3.3.1 Sensitivity

When adsorption of surfactants at an LC-aqueous interface exceeds a critical value, an ordering transition occurs. A lower critical transition value indicates greater sensitivity; therefore, the critical transition value was used as an indicator of the performance of this system. We studied the optical appearance when microcapillary-confined LCs contacted three surfactant solutions (CTAB, SDS, and sodium oleate) at various concentrations (10 µM – 10 mM). The lower concentration solutions were prepared by serial dilution. We took all the optical images after inserting a full wave retardation plate to enhance contrast in weak birefringence. When the concentration of the CTAB or SDS solution was >100 µM, the LCs displayed the four-petal texture, indicating that enough surfactants had absorbed at the LC-aqueous interface to trigger the orientation transition. Two bright lines were observed at concentrations <50 µM (Figure 3). These observations demonstrate that the critical ordering transition concentration for CTAB and SDS is between 100 and 50 µM in this microcapillary-confined LC sensing system. The critical transition concentration for sodium oleate was found to be between 1 mM and 100 µM. In comparison, the critical transition value for LC thin film systems is 0.32 mM for SDS[16]. Thus, the present experimental imaging system was more sensitive than existing thin film systems.

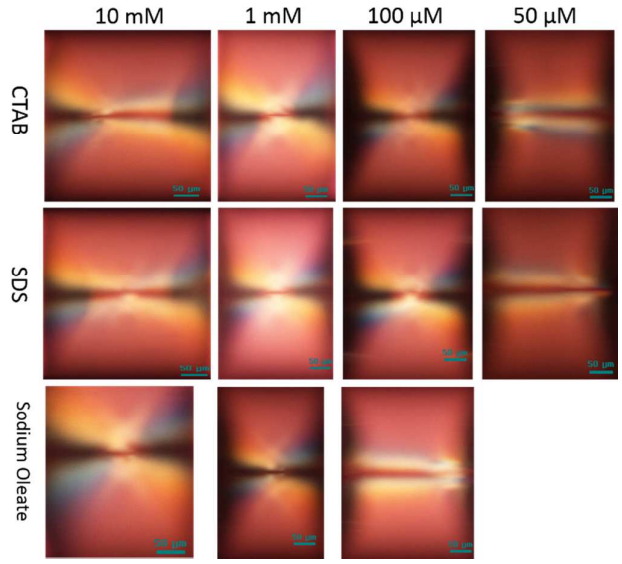

Figure 3. Polarized optical images of LCs contacting CTAB, SDS, and sodium oleate at various concentrations. The detection limit for CTAB and SDS was between 50 and 100 µM and that of sodium oleate was between 100 µM and 1 mM. The scale bar represents for 50µm.

3.3.2 Stability of the LC textures

The present microcapillary-based system has at least two advantages that greatly increase stability. Only the two ends of the microcapillary are open to the environment and the capillary is small (inner diameter, 400 µm), so the contact area is also small, reducing evaporation. In addition, in the microcapillary, the LC droplets and solution alternate and the LCs are non-volatile. Thus, the LCs prevent evaporation of the solutions. Due to these advantages, we expected the present imaging system to be quite stable. We studied the stability of the LC textures formed in the microcapillary in contact with CTAB (1 mM) and DI water, representing surfactant and non-surfactant solutions, respectively. After 120 h (5 days), the optical appearance remained the same (Figure 4). This strong stability suggests that this microcapillary-confined LC imaging system has great promise.

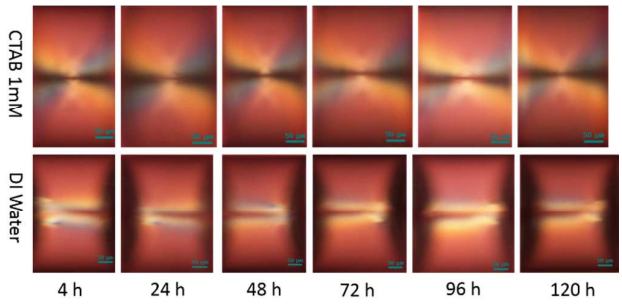

Figure 4. The LC textures formed in the microcapillaries were stable for more than 120 h. The scale bar represents for 50µm.

3.3.3 Reusability of the OTS-treated capillary

One of the drawbacks of thin film systems is that they cannot be reused. If a sensing system were reusable, that would save money, materials, and human resources. We studied the reusability of the OTS-treated microcapillaries by cleaning the used microcapillaries with DI water, drying them in an oven (37 °C), then using them again. We verified reusability for 10 "use-clean-dry" cycles (LC contact with 1 mM CTAB) (Figure 5), and concluded that the OTS-treated microcapillaries can be reused at least 10 times without significant effects.

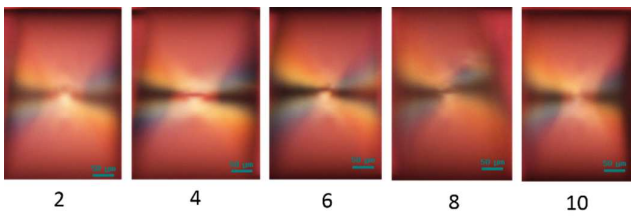

Figure 5. The OTS-treated microcapillaries can be used at least 10 times. The scale bar represents for 50µm.

3.4 Imaging application

Lipids were once regarded as an inert matrix, due to their low reactivity. Recently, studies have increasingly shown that lipids are an active interface having specific interactions with different types of molecules. Electrostatic interactions between cations and lipid molecules produce key structural and dynamic changes in polar head groups. Bivalent metal ions are essential to numerous life processes. They interact with cell membranes, modifying their conformation, structure, and stability. In addition, bivalent metal ions play a key role in membrane fusion processes[26]. Phospholipids interact strongly with bivalent metal ions at low concentrations (0.1–1 mM) to form metal ion–phospholipid complexes[28]. Here, we used the microcapillary-confined system to study interactions between phospholipid vesicles and bivalent metal ions, as one example of how the present system could be applied to study liquid-liquid interfacial phenomena. We first studied changes in the optical images of the microcapillary-confined LCs with DOPG concentration. We diluted the prepared DOPG solution (2 mM) to 0.5 mM, 0.2 mM, 0.15 mM, and 0.1 mM and introduced these DOPG solutions into microcapillary-confined LCs. The critical transition point of DOPG was observed to be between 0.15 mM and 0.2 mM (Figure 6). Specifically, when the concentration of DOPG was >0.2 mM, the four-petal texture was observed, while at concentrations <0.15 mM, two bright lines were displayed. We then studied the interaction between DOPG vesicles (0.15 mM) and bivalent metal ions (9.2 mM of Ca^{2+}, Co^{2+}, Cu^{2+}, Mg^{2+}, Pb^{2+}, or Fe^{2+}) (Figure 6). As noted above, when the 0.15 mM DOPG solution contacted the LC, two bright lines were observed. However, when DOPG solutions (0.15 mM) with bivalent metal ions (Ca^{2+}, Co^{2+}, Cu^{2+}, Mg^{2+}, or Pb^{2+}) contacted the microcapillary-confined LC, we observed the four-petal texture, indicating that more surfactants were absorbed at the LC-aqueous interface. Two mechanisms may be responsible for this behavior. The formed metal ion–phospholipid complexes may be absorbed at the interface more easily or the metal ions may increase lipid organization, inducing interfacial packing of monolayers[27]. However, when the DOPG Fe^{2+} solution was introduced, the four-petal texture did not appear, suggesting that DOPG and Fe^{2+} cannot form a metal ion–phospholipid complex. This could be confirmed by the Fenton reaction of phospholipids[26]. In conclusion, LCs confined in the microcapillary sensing system can be used to study the interactions of phospholipids and bivalent metal ions at LC-water interfaces.

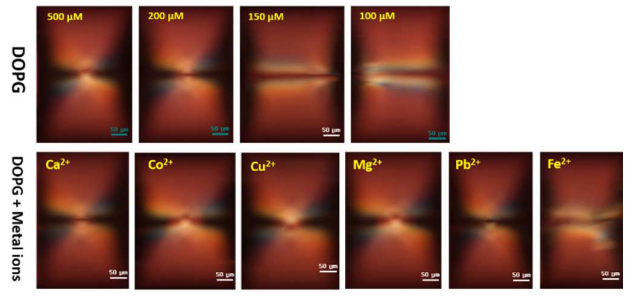

Figure 6. The top row shows polarized microscope images of LCs contacting DOPG at various concentrations. When the concentration was ≤150 μM, the characteristic image of two bright lines was observed. The bottom row shows images of LCs contacting DOPG (150 μM) and bivalent metal ions (Ca^{2+}, Co^{2+}, Cu^{2+}, Mg^{2+}, Pb^{2+}, or Fe^{2+}). The four-petal textures were observed, except with DOPG and Fe^{2+}. The scale bar represents for 50μm.

4 Conclusions

In summary, we developed a novel experimental imaging system based on nematic LCs confined in microcapillaries, which compared to LC thin film systems are smaller and more sensitive. The optical textures formed in the microcapillaries are stable for more than 120 h and the OTS-treated microcapillaries can be reused at least 10 times. In addition, the system is portable and easily fabricated. The LCs showed distinctive optical images before and after adsorption of amphiphiles at LC-water interfaces. Specifically, before adsorption of surfactants, two bright lines appeared, while a four-petal texture was observed after adsorption of surfactants. Furthermore, we successfully applied our system to monitor interactions between phospholipids and metal ions, suggesting that it can be broadly applied to report liquid-liquid interfacial phenomena. Because each microcapillary-confined LC droplet has two LC-water interfaces, we also conclude that the system could be used with an experimental group at one interface and a control group at the other interface at the same time and under exactly the same conditions.

Acknowledgements

This study was supported by a grant from the Korean Health Technology R&D Project, Ministry of Health & Welfare, Republic of Korea (HI13C0891) and the Basic Science Research Program through the National Research Foundation of Korea (NRF) funded by the Ministry of Science, ICT & Future Planning (NRF-2013R1A1A1A05008333).

Notes and references

1 L. Schmidt-Mende, a Fechtenkötter, K. Müllen, E. Moons, R. H. Friend, J. D. MacKenzie, Science 2001, **293**, 1119–1122.
2 H. Coles, S. Morris, Nat. Photonics 2010, **4**, 676–685.
3 D. C. Zografopoulos, R. Asquini, E. E. Kriezis, a d'Alessandro, R. Beccherelli, Lab Chip 2012, **12**, 3598–610.
4 F. Du, Y.-Q. Lu, S.-T. Wu, Appl. Phys. Lett. 2004, **85**, 2181.
5 I. W. Hamley, V. Castelletto, Z. B. Lu, C. T. Imrie, T. Itoh, M. Al-Hussein, Macromolecules 2004, **37**, 4798–4807.
6 M. A. Gharbi, M. Nobili, M. In, G. Prévot, P. Galatola, J.-B. Fournier, C. Blanc, Soft Matter 2011, **7**, 1467.
7 F. C. Keber, E. Loiseau, T. Sanchez, S. J. Decamp, L. Giomi, M. J. Bowick, M. C. Marchetti, Z. Dogic, A. R. Bausch, Science 2014, **345**, 1135–1140.
8 T. Sanchez, D. T. N. Chen, S. J. DeCamp, M. Heymann, Z. Dogic, Nature 2012, **491**, 431–4.
9 V. Schaller, C. Weber, C. Semmrich, E. Frey, A. R. Bausch, Nature 2010, **467**, 73–77.
10 A. Sengupta, U. Tkalec, M. Ravnik, J. Yeomans, C. Bahr, S. Herminghaus, Phys. Rev. Lett. 2013, **110**, 048303.
11 Y. H. Kim, D. K. Yoon, H. S. Jeong, O. D. Lavrentovich, H.-T. Jung, Adv. Funct. Mater. 2011, **21**, 610–627.
12 J. Fukuda, S. Zumer, Nat. Commun. 2011, **2**, 246.

13 S. Zhong, C.-H. Jang, Biosens. Bioelectron. 2014, **59**, 293–299.
14 X. Bi, D. Hartono, K.-L. Yang, Adv. Funct. Mater. 2009, **19**, 3760–3765.
15 Y. Liu, D. Cheng, I.-H. Lin, N. L. Abbott, H. Jiang, Lab Chip 2012, **12**, 3746–53.
16 J. Brake, N. Abbott, Langmuir 2002, **18**, 6101–6109.
17 J. M. Brake, M. K. Daschner, Y.-Y. Luk, N. L. Abbott, Science 2003, **302**, 2094–7.
18 D. Hartono, C. Y. Xue, K. L. Yang, L. Y. L. Yung, Adv. Funct. Mater. 2009, **19**, 3574–3579.
19 J.-S. Park, N. L. Abbott, Adv. Mater. 2008, **20**, 1185–1190.
20 Y. Wang, Q.-Z. Hu, Y. Guo, L. Yu, Biosens Bioelectron. 2015, **72**, 25-30
21 CY. Chang, CH. Chen, Chem. Commun., 2014, **50**, 12162-5.
22 A. D. Price, D. K. Schwartz, J. Am. Chem. Soc. 2008, **130**, 8188–8194.
23 A. D. Price, D. K. Schwartz, J. Phys. Chem. B 2007, **111**, 1007–15.
24 Q.-Z. Hu, C.-H. Jang, Colloids Surf. B. Biointerfaces 2011, **88**, 622–6.
25 Q.-Z. Hu, C.-H. Jang, Soft Matter, 2013, **9**, 5779
26 M. Zhang, C.-H. Jang, J. Biosci. Bioeng. 2015, doi:10.1016/j.jbiosc.2014.12.016
27 M. Prudent, M. a Méndez, D. F. Jana, C. Corminboeuf, H. H. Girault, Metallomics 2010, **2**, 400–406.
28 D. Papahadjopoulos, Biochim. Biophys. Acta 1968, **163**, 240–254.